DOI: 10.1002/fuce.201400041

Microbial Power-Generating Capabilities on Micro-/Nano-Structured Anodes in Micro-Sized Microbial Fuel Cells

A. Fraiwan[1], S. P. Adusumilli[2], D. Han[3], A. J. Steckl[3], D. F. Call[4], C. R. Westgate[2], S. Choi[1]*

[1] Bioelectronics & Microsystems Lab, Department of Electrical & Computer Engineering, State University of New York-Binghamton, Binghamton, NY 13902, USA
[2] Center for Autonomous Solar Power, State University of New York-Binghamton, Binghamton, NY 13902, USA
[3] Nanoelectronics Laboratory, Department of Electrical Engineering & Computing Systems, University of Cincinnati, Cincinnati, OH 45221, USA
[4] Department of Civil Construction and Environmental Engineering, North Carolina State University, Raleigh, NC 27695, USA

Received March 17, 2014; accepted August 01, 2014; published online ■■■

Abstract

Microbial fuel cells (MFCs) are an alternative electricity generating technology and efficient method for removing organic material from wastewater. Their low power densities, however, hinder practical applications. A primary limitation in these systems is the anode. The chemical makeup and surface area of the anode influences bacterial respiration rates and in turn, electricity generation. Some of the highest power densities have been reported using large surface area anodes, but due to variable chemical/physical factors (e.g., solution chemistry, architecture) among these studies, meaningful comparisons are difficult to make. In this work, we compare under identical conditions six micro/nano-structured anodes in micro-sized MFCs (47 μL). The six materials investigated include carbon nanotube (CNT), carbon nanofiber (CNF), gold/poly (ε-caprolactone) microfiber (GPM), gold/poly(ε-caprolactone) nanofiber (GPN), planar gold (PG), and conventional carbon paper (CP). The MFCs using three dimensional anode structures (CNT, CNF, GPM, and GPN) exhibited lower internal resistances than the macroscopic CP and two-dimensional PG anodes. However, those novel anode materials suffered from major issues such as high activation loss and instability for long-term operation, causing an enduring problem in creating widespread commercial MFC applications. The reported work provides an in-depth understanding of the interplay between micro-/nano-structured anodes and active microbial biofilm, suggesting future directions of those novel anode materials for MFC technologies.

Keywords: Biofilm Formation, Extracellular Electron Transfer, Mass Transfer, Micro-/Nano-Structured Anode Materials, Microbial Fuel Cell

1 Introduction

The last three decades have witnessed significant developments and performance improvements in microbial fuel cell (MFC) technology [1]. These advances are reflected in an increasing number of scientific publications and patents [2, 3]. MFCs are seen as a promising alternative technology that could alleviate the energy crisis and environmental pollution [4]. For this reason, MFCs have provided a focus for renewable energy production research. Despite advances, however, the promise of this technology has not yet been translated into commercial reality, because existing MFCs demonstrate low power density [5, 6]. Aside from all the other factors affecting the MFC performance such as bacterial inoculums, chemical substrates, ion-selective membranes, and reactor configuration [7], the anode materials play a profound role in influencing the power generation by determining: (i) the actual accessible area for bacteria to attach; (ii) the extracellular electron transfer efficiencies; and (iii) chemical species diffusion rates [8–10]. Therefore, many of the studies to date have concentrated on improving anode performance by the search for effective anode material and/or modifications to the anode surface [11–14]. Recently, many unconventional three-dimensional micro-/nano-scale and/or micro-fabricated anode materials

[*] *Corresponding author, sechoi@binghamton.edu*

have been explored to increase surface area, porosity, biocompatibility, conductivity, and biofilm formation [8–10, 15].

Gold has been proposed as a potential anode material because it is biocompatible, highly conductive and is compatible with conventional microfabrication modalities for the development of a micro-sized MFC platform [16, 17]. Choi and Chae [18] developed a microfabricated gold anode MFC generating about 100 $\mu W\,cm^{-2}$ with *Geobacter*-enriched mixed bacterial culture. Also, one-dimensional nanomaterials have attracted much attention due to their larger surface area and greater permeability. Qiao et al. [19] proposed a nanostructured polyaniline (PANI)/mesoporous TIO_2 composite anode in *Escherichia coli* MFCs. This new hybrid polymer/inorganic porous composite provided a large specific surface area, uniform nanopore distribution, and good biocatalytic performance, generating ~150 $\mu W\,cm^{-2}$. Zhang et al. [20] developed a graphene modified stainless steel mesh anode for the MFCs, generating ~270 $\mu W\,cm^{-2}$ with *E. coli.* Xie et al. [9, 21] introduced several three-dimensional anodes prepared by coating macroscale porous substrates with single-walled carbon nanotubes (CNT) or graphene. Their MFCs equipped with these anode materials and mixed bacterial culture achieved high power densities and lower energy losses than traditional carbon-based anodes, delivering 110 and 160 $\mu W\,cm^{-2}$, respectively. Choi and colleagues [15] reported a microfabricated anode based on gold coated poly(ε-caprolactone) (PCL) microfiber that outperformed a gold microelectrode by a factor of 2.65-fold and even carbon paper (CP) by 1.39-fold. All of these novel micro-/nano-structured anodes reported to date showed higher conductivity and mechanical stability with larger surface area and higher electrochemical catalytic activity compared to the conventional carbon-based materials such as graphites, carbon clothes, CP, and reticulated vitrified carbons [11, 12, 21]. However, their performances are often more dependent on the specific MFC architecture (e.g., chamber geometry, single or dual chamber), electrode spacing, environmental conditions (e.g., temperature, pH, and humidity), operating conditions (e.g., batch-mode or continuous mode), cathode materials, solution ionic strength, and conductivity of the fuel cells [22, 23]. Therefore, power densities produced by a certain anode in one study cannot be directly compared with another anode unless the MFC architecture, bacteria, and chemical solution are the same. Moreover, the anode chamber volumes employed for those studies range from several mL to L. This limits the accuracy, reproducibility, and reliability, due to large background current noise, and large variations in microbial growth, competition, and metabolisms of the consortium of microbes [24]. In addition, most of these anode studies for improving the MFC anode performances did not provide long-term analyses beyond 10 days even though microbial communities and their electron generating capabilities on anode materials will likely be affected by long-term operation. Therefore, the studies on micro-/nano-structured anode materials reported to date would not provide useful information unless the results are compared under the same conditions for a long period of time (>1 month).

Here, we compared six popular micro- and nano-structured anode materials in 47 μL micro-sized MFCs under the same experimental conditions for 1 month. The six anodes are carbon nanotubes (CNT), carbon nanofiber (CNF), gold/poly(ε-caprolactone) microfiber (GPM), gold/poly(ε-caprolactone) nanofiber (GPN), planar gold (PG), and conventional carbon paper (CP). CNT and CNF are emerging nanomaterials with higher mechanical strength and electrical conductivity than conventional carbon-based materials (CP). Also, non-carbon polymers with conductive materials (such as gold, CNT, and nanocomposites) have become one of the anode materials with high potential because of their large specific surface area and excellent stability. In particular, PCL is a well-known biopolymer, which can be easily prepared by electrospinning technique. The biofilm profiles, activation loss, internal resistances, and mass transfer losses on each anode material are thoroughly analyzed. The reported work will provide an in-depth understanding of the interplay between micro-/nano-structured anodes and active microbial biofilm, suggesting future directions of those novel anode materials for MFC technologies.

2 Materials and Methods

2.1 Device Fabrication and Assembly

A compact and reliable micro-liter sized MFC was prepared with each anode (Figure 1). The MFC contains vertically stacked 47 μL anode and cathode chambers separated by a PEM (Nafion 117) (Figure 1a). Each layer except for the PEM was micro-patterned using laser micromachining (Universal Laser Systems VLS 3.5). Each chamber volume was defined by 0.158 cm-thick patterned poly(methyl methacrylate) (PMMA) and 100 μm-thick thin plastic gasket. The exposed anode/cathode area was 0.28 cm^2. The Nafion 117 was sandwiched by the two PMMA chambers and thermally bonded at 125 °C for 1 h. We fabricated 4 cm × 6.2 cm PMMA supporting frames (0.5 inch thick) with the laser engraver and drilled six holes for fluidic inlet/outlet and screws (Figure 1b). In order to maintain consistency of experimental procedures, gold was used as a cathode material for all tests. The cathodes were prepared by depositing 100 nm gold on PMMA substrates with chrome (20 nm) as the adhesion layer. Six micro-sized MFCs were prepared with different anode materials; CNT, CNF, gold/PCL microfiber (GPM), gold/PCL nanofiber (GPN), PG, and conventional CP. Before we assembled the MFC, the anode/cathode chips were first sterilized with 70% ethanol and then blown dry with nitrogen. All layers were manually stacked in sequence while carefully aligning the tubing holes for the microfluidic channels. Four tubes (CODAN, 0.35 mL volume) were plugged into the holes to form two independent routes for anolyte/catholyte access. Copper tape (3M™ copper conductive tape) was attached to the contact pads with silver conductive paint (PELCO® Colloidal Silver).

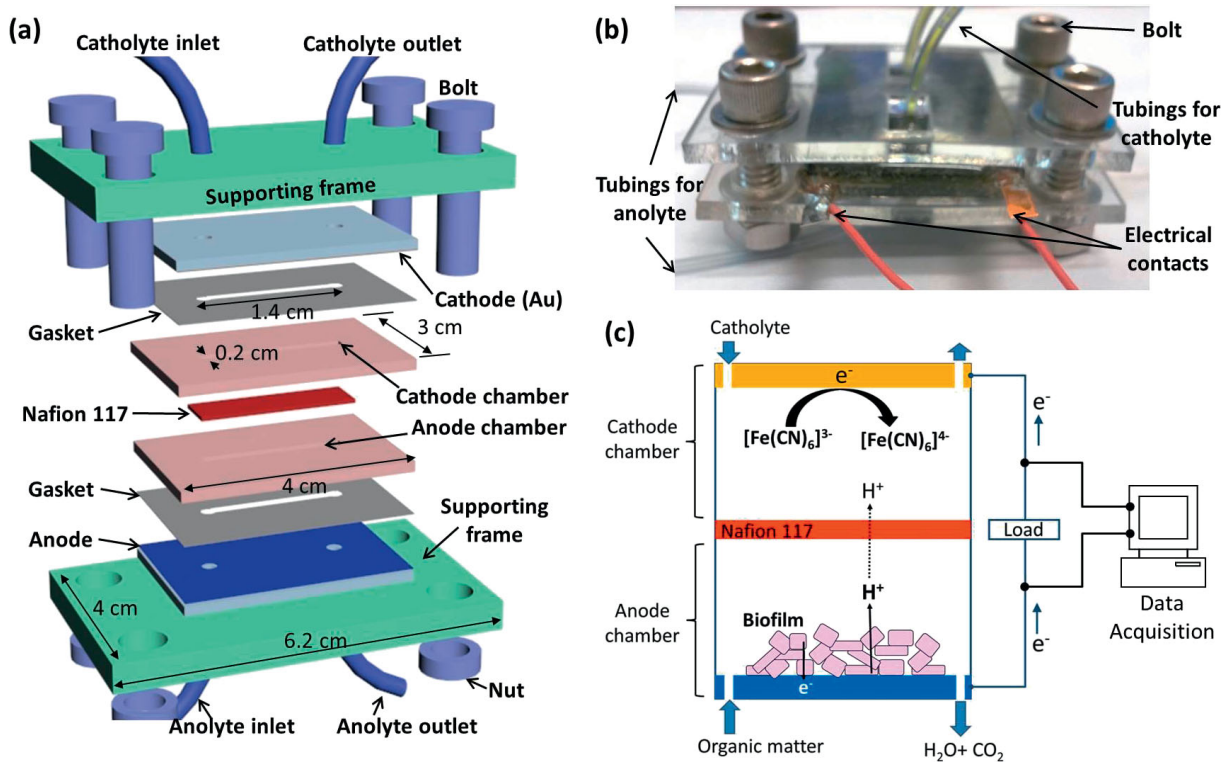

Fig. 1 (a) Schematic of the microfabricated MFC, (b) photograph of the fully assembled MFC, and (c) principles of operation of the MFC.

2.2 CNT and CNF Fabrication

Both CNTs and CNFs are grown through the diffusion of carbon via a transition metal catalyst (Ni, Co, and Fe). The carbon is obtained after the decomposition of the carbon source gas/liquid (methane, ethylene, and ethanol). The major distinction between CNTs and CNFs is based on the arrangement of the graphene layer, which is well described by Teo et al. [25]. In CNTs, the graphene layers act as parallel walls to the axis and in CNFs, the graphene layers are in an angle with the axis looking like graphene attached together. Quartz was used as the substrate. A 60 nm thick aluminum oxide (Al_2O_3) layer was deposited by atomic layer deposition (ALD) and a 5–15 nm thick Fe layer was deposited by thermal evaporation as shown in Supplementary Figure S1 [25, 26]. The substrate was placed inside the quartz tube in atmospheric pressure chemical vapor deposition (AP-CVD) setup and flushed by argon gas for 30 min. Then the furnace was turned on to the desired temperature (800 °C). Hydrogen flow of 10 sccm and argon flow of 200 sccm were passed through the tube. When the temperature reached the set temperature, the flow of ethylene was initiated, and after 2 min of ethylene flow, the water molecules were released from the bubbler through argon gas in the range of 150–400 sccm. After 60 min of growth time, the furnace, ethylene flow, and water flow were turned off and the furnace was cooled to 20 °C in 20 min. For CNFs, the synthesis setup was a little bit different from CNTs. Ni was used as the catalyst and deposited on Al_2O_3 coated quartz substrate by using DC sputtering. Synthesis of CNFs using catalytic decomposition was well described by Dr. Rodriguez (Supplementary Figure S2) [27].

2.3 GPM and GPN Fabrication

PCL fibers were prepared by electrospinning, a versatile technique to produce nano/microfiber membrane because of its excellent dimensional controllability, highly porous nonwoven structure, extremely high surface area to volume ratio, wide variety of materials, one-step production of multi-coated nano/microfibers, etc. In particular, the extremely high surface area and porous structure can lead to increased interaction with bacteria and, therefore, increased current density of MFCs. In this study, we have used PCL (Sigma–Aldrich, MW- = 90 KDa) as a fiber material, which has good biocompatibility and mechanical stability. To fabricate PCL microfiber membranes for the GPM device, the polymer solution (40 µL) dissolving 10 wt.% of PCL in 2,2,2-trifluoroethanol (TFE) (Acros Organics, 99.8% purity) solvent was constantly fed at 1.2 mL-h^{-1} by a syringe pump. High voltage ~12 kV was applied across a gap of 20 cm between the needle and the collector. Surfactants and/or ionic salts have been widely used to produce nanofiber membranes due to the increased charge density of the polymer solution. However, any additives lead to negative effects on a bacteria culture, hindering MFCs performance significantly. To fabricate PCL nanofiber sample for GPN device without any additives, PCL solution was prepared by dissolving 25 wt% of PCL into a highly ionic formic acid (Acros Organics, 88% purity). This solution was fed at 0.1 mL h^{-1} and the high voltage of 24 kV was applied across a gap of 25 cm. Because of very vigorous whipping and stretching actions of the ejected liquid jet, solidified fibers were attached to the collector. After electrospinning, the collected fiber mats

were dried in a vacuum oven for 12 h to remove any residual solvent. For gold coating on PCL electrospun fiber mats, sputtered gold was deposited on fibers for 10 min using Desk II mini-sputter system (Denton).

2.4 CP and PG Fabrication

CP (Fuel Cell Store, 0.48 g cc^{-1}, 0.2 mm) was cut into 3 cm × 4 cm pieces and put on the PMMA. The PG was prepared by depositing 100 nm gold on the PMMA substrate with chrome as the adhesion layer.

2.5 Measurement Setup

We measured the potential between the anode and the cathode by a data acquisition system (NI, USB-6212) and recorded the results every 1 min via a customized LabVIEW interface. An external resistor was used to close the circuit by connecting the anode and cathode. The current through the load was calculated via Ohm's law and the output power was calculated via $P = V \times I$. Current and power densities were normalized to the anode area.

2.6 Anolyte and Catholyte

We obtained pre-acclimated anode-respiring bacteria from an acetate-fed MFC initially inoculated with primary clarifier influent and operated for several months. We fed the anode chamber with acetate (1 g L^{-1} in mineral medium) as the sole electron donor. The catholyte was 100 mM ferricyanide in a 100 mM phosphate buffer in which the pH was adjusted at 7.5 ± 0.2 with 0.1 M NaOH. Electrons transferred to the anode via the bacterial conductive matrix flow to the cathode through the external resistor (Figure 1c). Protons travel through the ion exchange membrane toward the cathode. The redox couple completes when captured electrons reduce ferricyanide $[Fe(CN)_6]^{3-}$ at the cathode.

2.7 Bacterial Fixation and SEM Imaging

The MFCs were disassembled, rinsed, and adherent bacteria on each anode were immediately fixed in 2% glutaraldehyde solution overnight at 4 °C. Samples were then dehydrated by serial, 5 min transfers through 50, 70, 80, 90, 95, and 100% ethanol. Fixed samples were examined using a FESEM (Supra 55 VP, Zeiss).

2.8 Bacterial Biofilm Formation and MFC Operation

To accumulate and acclimate bacteria on the anode of MFCs, mixed bacterial culture and potassium ferricyanide were slowly injected into the micro-sized anode and cathode chambers, respectively. Open circuit and subsequent close circuit continuous experiments were run for 10 and 30 days, respectively, in micro-sized MFCs. The method of acclimatization for bacterial biofilms to populate an anode surface affects the type of bacteria grown on the anode and their viability from the anode, determining overall bacterial electron transfer capabilities [28–30]. The purpose of acclimatization is to maximize biofilm formation and increase electricity generation. There are four acclimatization methods commonly used in the literature; (i) open circuit, (ii) closed circuit, (iii) controlled cell potential between the anode and cathode compared to the reference electrode, and (iv) controlled anode potential between the anode and reference electrode [28]. Open circuit and closed circuit operations are the simplest techniques to accumulate and acclimate bacterial biofilms on the anode [28, 31]. Open circuit allows the biofilm formation to develop a steady-state open circuit voltage (OCV) utilizing natural redox processes in the environment while closed circuit operation allows the biofilm to reach a steady-state electron transfer. Controlled cell and anode potential control methods require external power through the reference electrode. Since the stability (lifetime) and miniaturization of the conventional planar Ag/AgCl reference electrodes are still insufficient to support long-term micro-sized MFC studies [32, 33], controlled potential acclimatization (conventional control method in macro-sized MFCs) is not applicable for the micro-sized MFCs. Instead, open circuit and closed circuit acclimation have been commonly used in the micro-sized MFC studies [18, 34]. For closed circuit operation, it is very important to choose the right external resistor that is equal to the MFC internal resistance in order to effectively operate the MFCs [35]. Also, differences in the external resistance may influence the MFC performance by affecting the biofilm structure in the anode and their metabolism [36, 37].

3 Results and Discussion

We first formed the biofilm under open circuit operation for 10 days and then, for the close circuit operation in order to firmly form the biofilm, chose the optimal external resistance, where the maximum power density can be generated. It is well known that open circuit acclimatization decreases biofilm viability primarily located at the inner layer of the biofilm because cell growth and metabolism inside biofilm layers nearer to the anode cannot be efficiently supported by electron acceptors (either oxygen or anode) [30, 38]. However, unviable biofilm domains can be fully recovered under the subsequent close circuit operation in the initial development of the biofilms [38].

OCVs of the micro-sized MFCs are shown in Figure 2. There are roughly three different stages evident, relating to formation of the microbial biofilm: (i) initial bacterial attachment; (ii) biofilm formation through exopolysaccharide substance; (iii) saturation releasing bacteria in the planktonic form and continuing the cycle again. Over the first day under open circuit operation, cell voltages significantly increased and followed by a slower increase until the MFCs maintained a constant cell voltage at around 7 days except for the CNT and CNF anodes that kept increasing even at 10 days. This is

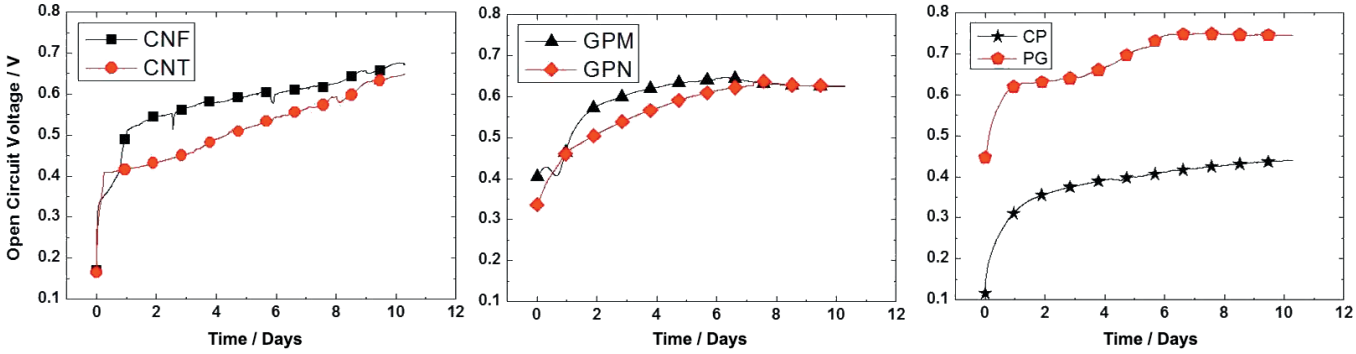

Fig. 2 Variation in voltage with time in micro-sized MFCs provided with six different micro-/nano-anodes materials running under open circuit.

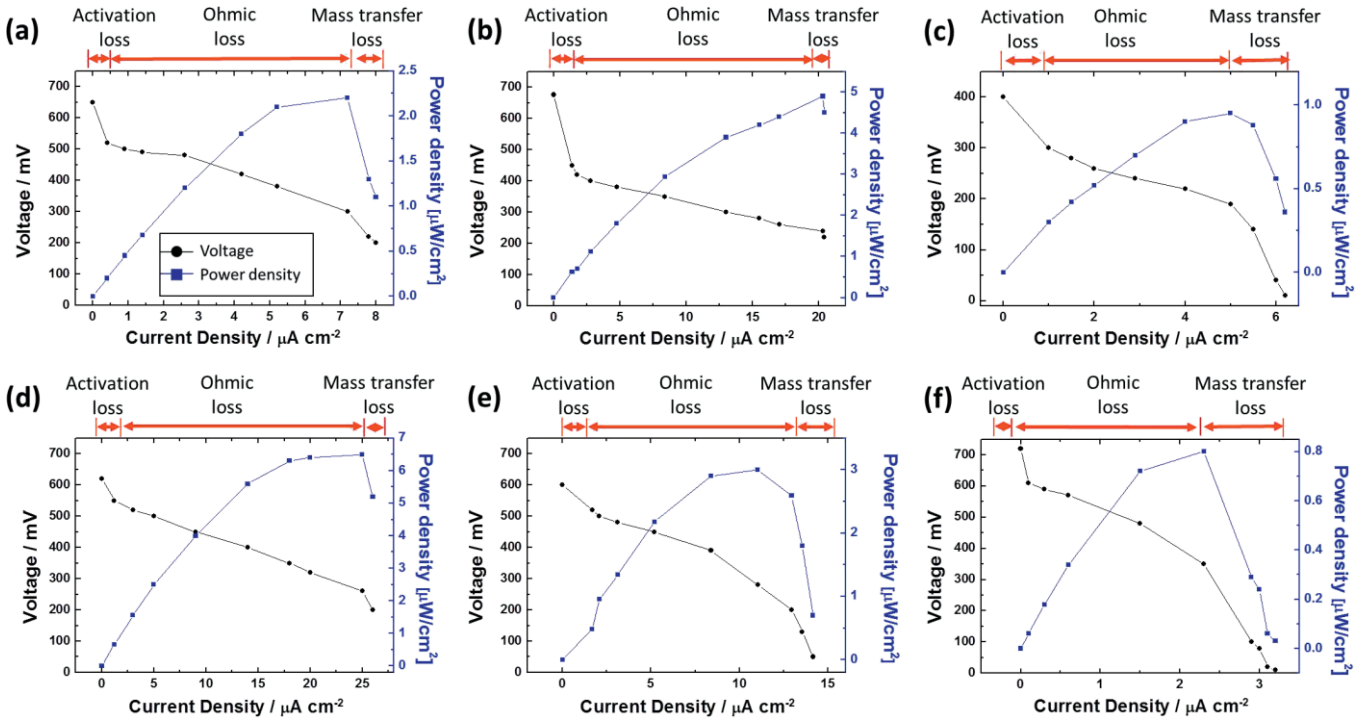

Fig. 3 Polarization curve (black circle) and power output (blue square) of the MFCs with six different anode materials, measured as a function of current; (a) CNF, (b) CNT, (c) CP, (d) GPM, (e) GPN, and (f) PG. The values are derived and calculated based on the maximum current value at a given external resistance (680 k, 470 k, 330 k, 220 k, 150 k, 100 k, 47 k, 22 k, 10 k, and 1 kΩ). The individual losses are divided into three zones according to their occurrence at different polarization levels; activation loss, ohmic loss, and mass transfer loss.

mainly because the biofilm formation was still being processed on the larger surface area. Accordingly, higher electrochemical catalytic activity was promoted compared to the other anode materials. After the MFCs were initially inoculated under open circuit operation for 10 days, cell polarization curves and power outputs of the six MFCs with different anode materials were derived and calculated based on the saturated current value at a given external resistance (680 k, 470 k, 330 k, 220 k, 150 k, 100 k, 47 k, 22 k, 10 k, and 1 kΩ) (Figure 3). Since we used 100 mM ferricyanide, corresponding to 100 e^- meq L^{-1}, which is far more than the number of electron equivalents available at the anode (~80 e^- meq L^{-1}) and the current generated from the MFCs are in the μA ranges, we ensured that the cathodic parts did not limit the process. In addition, the cathode materials/experimental conditions are the same in all MFCs and the sufficient ferricyanide supply kept the cathode potential constant during the experiments. Therefore, the results produced from the micro-sized MFC were enough only for studies on effects of the anode materials on MFC performances. Using the polarization curve, the major electrochemical losses in MFCs can be analyzed. The individual losses are divided into three zones according to their occurrence at different polarization levels indicated in Figure 3; activation loss region (starting from the OCV at zero current, there is an initial steep decrease of the voltage), ohmic loss region (the voltage then falls more slowly and the voltage drop is linear with current), and mass transfer loss region (there is a rapid decline of the voltage at higher currents). These losses can be defined by the voltage increase required to compensate for the current loss due to electrochemical reac-

ORIGINAL RESEARCH PAPER

tions, charge transport, and mass transfer processes that take place in different anode materials [39]. Using the polarization curve, we also estimated internal resistances from the ohmic loss regions (linear fitting of the curve), which agree well with the external resistor values where the maximum power density is obtained in Figure 3. The optimal external resistors obtained from Figure 3 were used to run the individual MFCs under close circuit operation (Figure 4) (optimal external resistors; CNF – 22 kΩΩ, CNT – 10 kΩ, CP – 4 kΩ, GPM – 10 kΩ, GPN – 47 kΩ, and PG – 100 kΩ). SEM images of all anodes from MFCs were taken before and after biofilm formation (Figure 5) in order to observe the morphologies and micro-/nano-pores of the anode surface and the presence of attached biofilms on each anode material. In addition, the SEM images

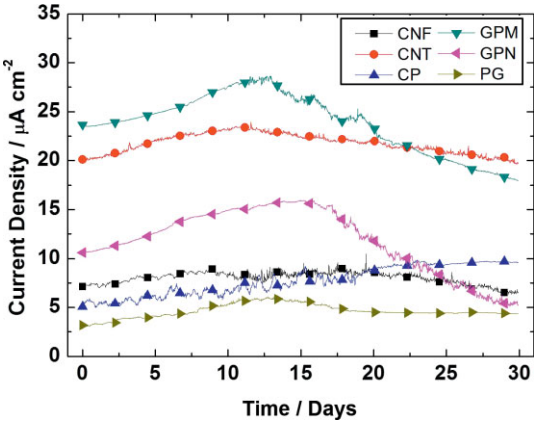

Fig. 4 Currents produced from the six MFCs having different anode materials with the optimal external resistors (optimal external resistors; CNF – 22 kΩ, CNT – 10 kΩ, CP – 4 kΩ, GPM – 10 kΩ, GPN – 47 kΩ, and PG – 100 kΩ).

relate the extent of biofilm coverage to the characteristics of the anodes and the different levels of performance measured from the different MFCs (Figures 3 and 4). All the numerical values obtained from Figures 3 and 4 are summarized in Table 1. Under the open circuit operation shown in Figure 2, the maximum OCVs obtained with CNT (680 mV), CNF (660 mV), GPM (620 mV), GPN (610 mV), and PG (720 mV) were greater than the CP (400 mV) (Table 1). Given that these OCV values are the cell voltages that indicate the difference between the potential under equilibrium conditions and the thermodynamic losses, the CP's OCV being substantially lower than the others clearly shows that there is a large energy loss occurring at the anode [7].

Activation losses are dominant at a low current density with high value of external resistors for all samples (680 and 470 kΩ) (Figure 3). Since an activation energy is required for the oxidation/reduction reaction, activation losses occur during the electron transfer from bacterial cells to the anode surface [40]. Therefore, the conductivity and surface area can be the main factors for the activation losses. However, despite their higher anode surface area (Figure 5), CNT- and CNF-based MFCs produced high activation losses (130 and 226 mV, respectively, shown in Figure 3 and Table 1) mainly due to their higher resistivity. Normally, gold-coated low resistance anode materials (GPM, GPN, and PG) had smaller activation losses even with lower surface area than CNT or CNF anodes. Based on these findings, the conductivity is the main determinant factor reducing activation losses.

In terms of the internal resistance, PG-based MFC showed the highest internal resistance (112 kΩ) while other three-dimensional micro-/nano-anodes and CP-based anode had lower resistance of 10–30 kΩ. Since the ohmic losses are

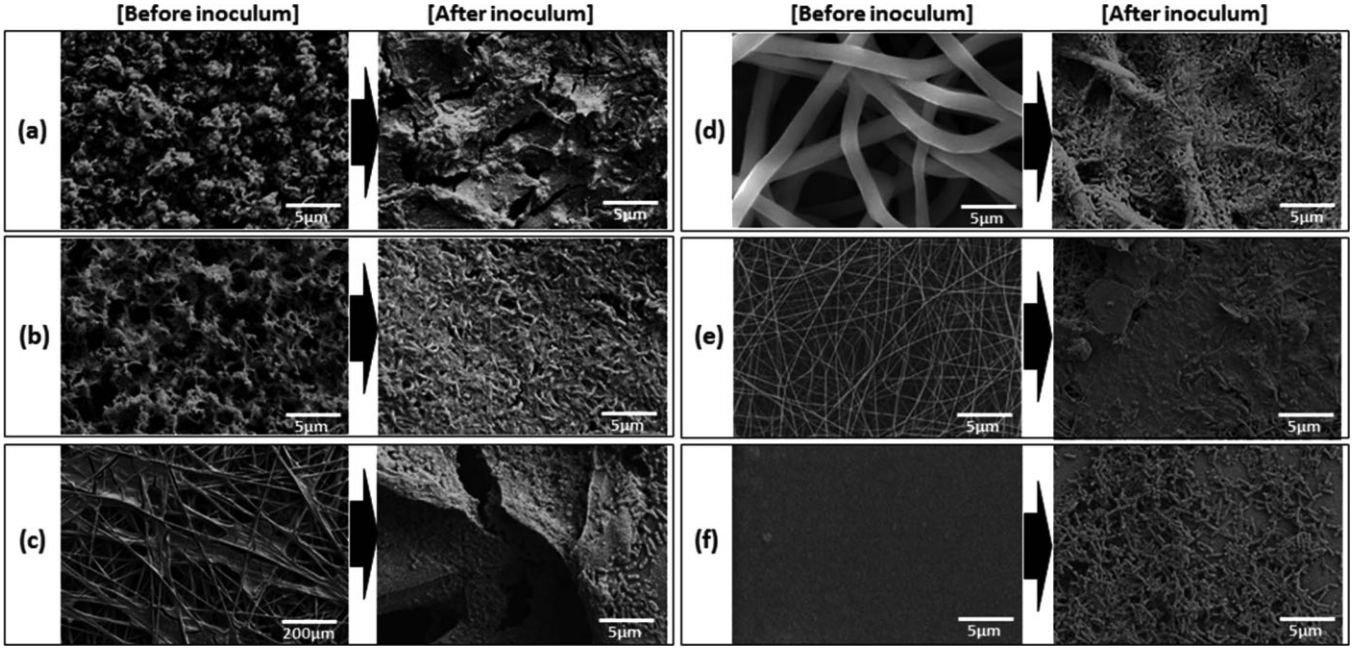

Fig. 5 SEM images of all anodes from MFCs before and after biofilm formation; (a) CNF, (b) CNT, (c) CP, (d) GPM, (e) GPN, and (f) PG (scale bar is shown).

Table 1 Overview of the resistivity, OCV, major electrochemical losses, and current/power densities during open circuit and closed circuit operations of the MFCs with different anode materials.

	Resistivity (Ω cm)	OCV (mV)	Activation loss (mV)	Internal resistance (kΩ)	Mass transfer loss (mV)	Open circuit operation		Closed circuit operation	
						Maximum power density ($\mu W\,cm^{-2}$)	Current density at optimal external resistance ($\mu A\,cm^{-2}$)	Maximum current density at optimal external resistance ($\mu A\,cm^{-2}$)	Final current density at 30 days
Carbon nanofiber (CNF)	0.25	660	~130	22	~100	2.2	7.2	8.3	6.5
Carbon nanotube (CNT)	0.33	680	~226	12	~50	4.9	20.1	23.4	19.8
Carbon paper (CP)	0.01	400	~100	30	~200	1.0	4.9	9.6	9.5
Gold/PCL microfiber (GPM)	0.01	620	~70	10	~60	6.5	24.8	28.5	18.0
Gold/PCL nanofiber (GPN)	0.02	610	~80	23	~170	2.9	11.7	15.8	5.4
Planar gold (PG)	0.001	720	~90	112	~350	0.8	2.4	5.8	4.3

strongly related to the resistance to the flow of ions through the proton exchange membrane, three-dimensional anodes (Figure 5) could be helpful for decreasing internal resistance. However, the internal resistances of the micro-sized MFCs are still much higher than that of macro-sized MFCs (a few Ω) [17]. This large discrepancy in internal resistance might be due to the accumulated protons in the biofilm and inefficient proton transfer, altering the redox conditions and hampering the metabolic activity of the biofilm [41]. Protons generated along with electrons during bacterial metabolism must move toward the bulk solution while electrons move toward the anode surface. Therefore, generally, slow proton transfer is the main limiting factor that affects the internal resistance of the MFC system. As the size of the MFC becomes smaller, it becomes extremely sensitive to inefficient proton transfer rate due to the reduced number of bacterial cells on the anodes compared to the macro-sized MFCs. Three dimensional anodes can allow for more efficient proton flux through the biofilm, decreasing the internal resistances.Mass transfer losses occur at high current densities when the mass transport rate of substrates limits current production (Figure 3 and Table 1). Limited mass transfer causes the occurrence of an anode saturation potential leading to voltage reversal with low external resistance. Actually, severe negative currents were observed from all MFCs under the 10 Ω external resistor. CNT- and GPM-based MFCs showed the lowest mass transfer loss (50 and 60 mV, respectively), while PG-based device had the highest voltage drop (350 mV) at high current densities indicating that three-dimensional materials allowed for efficient mass transport maximizing fluid flow toward and out of the micro-pores.

Subsequent closed circuit operation for long time would be helpful to understand system stability and anode performance for practical applications (Figure 4). Moreover, additional current increase under closed circuit operation to the value measured in polarization (Figure 3) indicates the viability recovery of biofilms formed under closed circuit. CNT, CNF, and GPM anodes with micro- or nano-pores showed only around 13% increase in current while CP, GPN, and PG anodes had 49, 30, and 59% increase from the current values measured in polarization (Figure 3 and Table 1) [30, 38]. The biofilm formed in open circuit operation includes an unviable domain in the inner layer of the biofilm because of the inefficient nutrient/oxygen/proton transfer. Switching into closed circuit operation could provide favorable electron acceptor and sufficient energy to support cell growth and metabolism inside the biofilms, recovering those unviable domains with increases in current. Larger current increases indicate that more unviable regions were recovered. Therefore, more than 85% of the biofilms formed on the CNF, CNT, and GPM anode materials even under open circuit operation can be viable because of their porosity distribution over the surface (Figure 5). For the long-term operation, CNT and CNF anodes reached a maximum current value within ~10 days, followed by a slight decrease for the next 10–15 days. This is possibly because of the cellular toxicity of carbon-based nanomaterials that could lead to proliferation inhibition and cell death [12]. Further research is required for this phenomenon. GPM and GPN anodes also showed similar current profiles to those of the carbon nanomaterials but with significant current drop from a peak value. This is mainly because of the poor gold adhesion and incomplete gold coverage on to the PCL fibers or likely biodegradable features of the fiber. The PG anode also experienced current decrease after 12 days. Although further studies are needed to examine this phenomenon, this must be related to the unfavorable bacterial attachment and incomplete biofilm formation (Figure 5). Further analysis is given in the next paragraph. The current of the CP anode increased more slowly and stabilized in 20 days. No current decrease was observed in ~ 30 days.

Anode materials and biofilm morphology on each anode were examined using SEM with results presented in Figure 5 and Supplementary Figure S3. In general, the images indicate that biofilms are fully formed on each anode surface, displaying rough uneven topography. The SEM results provide good comparative information demonstrating clear differences in the architectures of the biofilm established on anode surfaces and MFC performances presented in Table 1. CNT and CNF anodes include nano-pores between densely packed CNT and CNF sheets, which seem to be too small for bacterial attachment deep inside the material. Instead, biofilms were formed

all over the CNT sheet with entire coverage while the ones on the CNF sheets had some cracks. This is because the average height variation of the CNT-electrode surface was about 11 µm within a small range, while CNF-electrode surface's height ranged significantly from 2 to 8 µm (Figure 5a and b, and Supplementary Figure S3). However, these nanoscopic high-porosity materials seem to provide efficient proton transfer and substrates through nano-pores underneath the fully formed biofilm corresponding to results with low internal resistance and mass transfer losses (Table 1). Conventional CP showed macroscopic pores (~50 to 100 µm) that allowed the transport and colonization of microorganisms deep inside the anode surface. However, the macroscopic porosity of the CP showed higher internal resistance and mass transfer loss than that of the nanoscopic porous materials. The morphology of the GPM and GPN materials is shown in Figure 5d and e. The non-woven textile fibers formed an open micro- or nano-scale porous structure. GPM had a fiber diameter of ~1.38 µm and large pore size, which allowed for bacterial cells to enter deep inside the material and entirely wrap the micro-fibers. On the contrary, GPN had much smaller pore size than bacterial cells with about 118 nm in the fiber diameter. The nano-porous GPN were fully covered by bacterial biofilms that seemed to clog the pores, leading to inefficient proton and substrate transfer. The GPN MFC's internal resistance and mass transfer loss were much larger than that of GPM and even those of CNT and CNF-based MFCs. SEM image of the planar gold (PG) surface showed that there is not a complete coverage with bacterial cells and the cells are not embedded within a full matrix of extracellular polymeric substances (EPS) while other materials clearly indicated EPS, suggesting that somehow bacterial biofilm formation on the PG surface was slower than those on other anode materials or the gold itself is not an optimal surface for bacterial cell attachment.

4 Conclusion

We show here a direct comparison among several high-surface area anode materials with different properties. Their maximum power density/current density, material/fabrication cost, biocompatibility, surface area, longevity, stability, resistivity, and their internal resistance are all critical factors in developing a high performance MFC for actual applications. Three-dimensional anode structures (CNT, CNF, GPM, and GPN) are more preferable to reduce the internal resistance of the MFCs and increase the nutrient/proton/oxygen transfer efficiency through the biofilm than the macroscopic CP and two-dimensional PG anodes. However, even those novel anode materials require improvements for use in MFC practical applications. The power density of the GPM and GPN was high during the initial biofilm formation but their current stability and lifetime for long-term operation will need to be significantly improved. Also, CNT- and CNF-based anodes will require surface modification with other chemicals or materials for reducing huge activation losses and cellular toxicity. The reported work provided an in-depth understanding of the interplay between micro-/nano-structured anodes and active microbial biofilm, suggesting future directions of those novel anode materials for MFC technologies.

Acknowledgment

We would like to thank the Nanofabrication Lab at SUNY-Binghamton for providing the fabrication facilities, and the Binghamton University Research Foundation for supporting this work. This work was also supported in part by S^3IP Small Grant Award.

References

[1] D. R. Lovley, *Annu. Rev. Microbiol.* **2012**, *66*, 391.
[2] B. E. Logan, J. M. Regan, *Environ. Sci. Technol.* **2006**, *40*, 5172.
[3] J. C. Biffinger, B. R. Ringeisen, *Recent Pat. Biotechnol.* **2008**, *2*, 150.
[4] B. E. Rittmann, *Biotechnol. Bioeng.* **2008**, *100*, 203.
[5] B. E. Logan, *Appl. Microbiol. Biotechnol.* **2010**, *85*, 1665.
[6] A. Rinaldi, B. Mecheri, V. Garavaglia, S. Licoccia, P. D. Nardo, *Energy Environ. Sci.* **2008**, *1*, 417.
[7] B. E. Logan, B. Hamelers, R. Rozendal, S. U. chroder, J. Keller, S. Freguia, P. Aelterman, W. Verstraete, K. Rabaey, *Environ. Sci. Technol.* **2006**, *40*, 5181.
[8] V. Flexer, J. Chen, B. C. Donose, P. Sherrell, G. G. Wallace, J. Keller, *Energy Environ. Sci.* **2013**, *6*, 1291.
[9] X. Xie, G. Yu, N. Liu, Z. Bao, C. S. Criddle, Y. Cui, *Energy Environ. Sci.* **2012**, *5*, 6862.
[10] J. E. Mink, M. M. Hussain, *ACS Nano* **2013**, *7*, 6921.
[11] V. Gadhamshetty, N. Koratkar, *Nano Energy* **2012**, *1*, 3.
[12] M. Ghasemi, W. R. W. Daud, S. H. A. Hassan, S. Oh, M. Ismail, M. Rahimnejad, J. M. Jahim, *J. Alloys Compd.* **2013**, *580*, 245.
[13] G. Gnana Kumar, V. G. S. Sarathi, K. S. Nahm, *Biosens. Bioelectron.* **2013**, *43*, 461.
[14] M. Zhou, M. Chi, J. Luo, H. He, T. Jin, *J. Power Sources* **2011**, *196*, 4427.
[15] A. Fraiwan, S. Sundermier, D. Han, A. Steckl, D. J. Hassett, S. Choi, *Fuel Cells* **2013**, *13*, 336.
[16] H. Richter, K. McCarthy, K. P. Nevin, J. P. Johnson, V. M. Rotello, D. R. Lovley, *Langmuir* **2008**, *24*, 4376.
[17] S. Choi, H.-S. Lee, Y. Yang, P. Parameswaran, C. I. Torres, B. E. Rittmann, J. Chae, *Lab Chip* **2011**, *11*, 1110.
[18] S. Choi, J. Chae, *Sens. Actuators A* **2013**, *195*, 206.
[19] Y. Qiao, S. Bao, C. M. Li, X. Cui, Z. Lu, J. Guo, *ACS Nano* **2008**, *2*, 113.
[20] Y. Zhang, G. Mo, X. Li, W. Zhang, J. Zhang, J. Ye, X. Huang, C. Yu, *J. Power Sources* **2011**, *196*, 5402.
[21] X. Xie, M. Ye, L. Hu, N. Liu, J. McDonough, W. Chen, H. N. Alshareef, C. S. Criddle, Y. Cui, *Energy Environ. Sci.* **2012**, *5*, 5265.
[22] J. Wei, P. Liang, X. Huang, *Bioresour. Technol.* **2011**, *102*, 9335.

[23] A. P. Borole, G. Reguera, B. Ringeisen, Z. Wang, Y. Feng, B. H. Kim, *Energy Environ. Sci.* **2011**, *4*, 4813.
[24] S. Mukherjee, S. Su, W. Panmanee, R. T. Irvin, D. J. Hassett, S. Choi, *Sens. Actuators A* **2013**, *201*, 532.
[25] K. Teo, C. Singh, M. Chhowalla, W. Milne, *Encycl. Nanosci. Nanotechnol.* **2004**, *1*, 665.
[26] S. P. Adusumilli, *M. S. Thesis*, State University of New York at Binghamton, **2010** (ISBN: 9781124411354).
[27] N. M. Rodriguez, *J. Mater. Res.* **1993**, *8*, 3233.
[28] J. Babauta, R. Renslow, Z. Lewandowski, H. Beyenal, *Biofouling* **2013**, *28*, 789.
[29] R. P. Ramasamy, Z. Ren, M. M. Mench, J. M. Regan, *Biotechnol. Bioeng.* **2008**, *101*, 101.
[30] S. T. Read, P. Dutta, P. L. Bond, J. Keller, K. Rabaey, *BMC Microbiol.* **2010**, *10*, 98.
[31] A. Larrosa-Guerrero, K. Scott, K. P. Katuri, C. Godinez, I. M. Head, T. Curtis, *Appl. Microbiol. Biotechnol.* **2010**, *87*, 1699.
[32] M. W. Shinwari, D. I. Zhitomirsky, A. Deen, P. R. Selvaganapathy, M. J. Deen, D. Landheer, *Sensors* **2010**, *10*, 1679.
[33] F. Qian, D. E. Morse, *Trends Biotechnol.* **2011**, *29*, 62.
[34] F. Qian, M. Baum, Q. Gu, D. E. Morse, *Lab Chip* **2009**, *9*, 3076.
[35] R. P. Pinto, B. Srinivasan, S. R. Guiot, B. Tartakovsky, *Water Res.* **2011**, *45*, 1571.
[36] D. Y. Lyon, F. Buret, T. M. Vogel, J. Monier, *Bioelectrochemistry* **2010**, *78*, 2.
[37] K. P. Katuri, K. Scott, I. M. Head, C. Picioreanu, T. P. Curtis, *Bioresour. Technol.* **2011**, *102*, 2758.
[38] Y. Yang, G. Sun, J. Guo, M. Xu, *Bioresour. Technol.* **2011**, *102*, 7093.
[39] K. Rabaey, W. Verstraete, *Trends Biotechnol.* **2005**, *23*, 291.
[40] P. Aelterman, S. Freguia, J. Keller, W. Verstraete, K. Rabaey, *Appl. Microbiol. Biotechnol.* **2008**, *78*, 409.
[41] R. S. Renslow, J. T. Babauta, P. D. Majors, H. Beyenal, *Energy Environ. Sci.* **2013**, *6*, 595.

